Evidence of adaptations of locomotor neural drive in response to enhanced intermuscular connectivity between the triceps surae muscles of the rat

Bernabei, Michel; van Dieën, Jaap H.; Maas, Huub

published in
Journal of Neurophysiology
2017

DOI (link to publisher)
10.1152/jn.00625.2016

J Neurophysiol 118: 1677–1689, 2017.
First published May 10, 2017; doi:10.1152/jn.00625.2016.

RESEARCH ARTICLE | *Spinal Control of Motor Outputs*

Evidence of adaptations of locomotor neural drive in response to enhanced intermuscular connectivity between the triceps surae muscles of the rat

Michel Bernabei, Jaap H. van Dieën, and Huub Maas
Department of Human Movement Sciences, Faculty of Behavioral and Movement Sciences, Vrije Universiteit Amsterdam, MOVE Research Institute Amsterdam, The Netherlands

Submitted 5 August 2016; accepted in final form 8 May 2017

Bernabei M, van Dieën JH, Maas H. Evidence of adaptations of locomotor neural drive in response to enhanced intermuscular connectivity between the triceps surae muscles of the rat. *J Neurophysiol* 118: 1677–1689, 2017. First published May 10, 2017; doi:10.1152/jn.00625.2016.—The aims of this study were to investigate changes *1*) in the coordination of activation of the triceps surae muscle group, and *2*) in muscle belly length of soleus (SO) and lateral gastrocnemius (LG) during locomotion (trotting) in response to increased stiffness of intermuscular connective tissues in the rat. We measured muscle activation and muscle belly lengths, as well as hindlimb kinematics, before and after an artificial enhancement of the connectivity between SO and LG muscles obtained by implanting a tissue-integrating surgical mesh at the muscles' interface. We found that SO muscle activation decreased to 62%, while activation of LG and medial gastrocnemius muscles increased to 134 and 125%, respectively, compared with the levels measured preintervention. Although secondary additional or amplified activation bursts were observed with enhanced connectivity, the primary pattern of activation over the stride and the burst duration were not affected by the intervention. Similar muscle length changes after manipulation were observed, suggesting that length feedback from spindle receptors within SO and LG was not affected by the connectivity enhancement. We conclude that peripheral mechanical constraints given by morphological (re)organization of connective tissues linking synergists are taken into account by the central nervous system. The observed shift in activity toward the gastrocnemius muscles after the intervention suggests that these larger muscles are preferentially recruited when the soleus has a similar mechanical disadvantage in that it produces an unwanted flexion moment around the knee.

NEW & NOTEWORTHY Connective tissue linkages between muscle-tendon units may act as an additional mechanical constraint on the musculoskeletal system, thereby reducing the spectrum of solutions for performing a motor task. We found that intermuscular coordination changes following intermuscular connectivity enhancement. Besides showing that the extent of such connectivity is taken into account by the central nervous system, our results suggest that recruitment of triceps surae muscles is governed by the moments produced at the ankle-knee joints.

soleus; gastrocnemius; muscle recruitment; connective tissues; coordination

THE PRESENCE OF mechanical connections between muscle-tendon units increases the number of peripheral constraints imposed on the musculoskeletal system, thereby reducing the number of possible solutions for performing a motor task. Although critical for understanding neural control of normal and pathological movement, the effects of such peripheral constraints on the recruitment pattern of synergistic muscles remain unclear.

Previous studies have shown that connective tissue structures at the muscle boundary (i.e., epimysium) can transmit forces from muscles to their surroundings bypassing their origin and insertion (Huijing 1999; Maas and Sandercock 2010). Evidence of this so called epimuscular myofascial force transmission has been reported for humans in vivo (Bojsen-Møller et al. 2010; Oda et al. 2007; Tian et al. 2012; Yaman et al. 2013) and for animals in situ (e.g., Huijing and Baan 2001; Maas et al. 2001). However, when testing under more physiological conditions, other animal studies found very limited force transmission via epimuscular pathways (Maas and Sandercock 2008; Tijs et al. 2015, 2016). In pathological conditions that involve increased amounts of connective tissues as a result of, for example, muscle-tendon injury (Silder et al. 2008, 2010) or surgical treatments (Smeulders et al. 2002; Smeulders and Kreulen 2007), the role of epimuscular pathways is likely enhanced.

We recently reported that scar tissues between the one-joint soleus (SO) and two-joint gastrocnemius (GA) muscles increases their mechanical coupling (Bernabei et al. 2017a). Does this affect the recruitment pattern of these muscles during movement? There are several mechanisms to be considered. First, we consider the size principle for motor unit recruitment (Henneman 1957). There is some evidence that this principle is applicable also across muscles with similar function like SO and GA (Sokoloff et al. 1999). In line with this, SO, which contains a large proportion of type-I motor units, is preferentially recruited during locomotion (Prilutsky et al. 1994). If muscle recruitment is determined only by the size principle, no changes in neuromuscular control with enhanced intermuscular coupling would be predicted. Second, we consider sensory feedback from muscle receptors. Part of muscle activity amplitude during the stance phase of walking seems feedback related (Donelan and Pearson 2004; Sinkjaer et al. 2000; Stein et al. 2000). Proprioceptive feedback is also important in adapting the timing of the central locomotor program to changes in task demands (Rossignol et al. 2006). Since length-dependent feedback from one muscle is affected by changes in length and relative position of neighboring muscles (Smilde et

Address for reprint requests and other correspondence: H. Maas, Van der Boechorststraat 9, 1081 Amsterdam, The Netherlands (e-mail: h.maas@vu.nl).

al. 2016), it is conceivable that changes in muscle length modulation and speed of contraction due to an increased muscle coupling would be sensed by muscle spindles, thereby priming adaptations in neural drive. Third, we consider optimizing motor control to joint moment requirements. Muscle stress and metabolic costs of activation can be minimized by coordinating the activation of one-joint and two-joint muscles (Mehta and Prilutsky 2014). Enhanced connectivity between SO and GA will cause the initially one-joint ankle extensor SO to produce also substantial moments around the knee joint (Bernabei et al. 2017a). Consequently, the preexistent recruitment pattern of these muscles may become suboptimal and, consequently, be adapted.

The primary aim of this study was to investigate changes in the coordination of activation of the triceps surae muscle group during locomotion in response to an increased stiffness of intermuscular connective tissues in the rat, induced by implanting a tissue-integrating mesh at the muscles' interface. For this purpose, SO, lateral gastrocnemius (LG), and medial gastrocnemius (MG) activation, together with muscle belly length changes and hindlimb kinematics, were measured during locomotion. We hypothesized that the increased stiffness of intermuscular connective tissues and, thus, the altered mechanical interaction between these muscles result in changes of muscle recruitment. As a secondary aim, we tested whether the length changes of SO and LG muscle bellies were altered, as this may have implications for the sensory feedback from these muscles. Preliminary results have been presented in abstract form (Bernabei et al. 2015).

METHODS

Electromyographic signals of SO, LG, and MG muscles, as well as length signals from SO and LG muscle bellies and hindlimb kinematics were obtained during level trotting on a treadmill with a nominal speed of 0.8 m/s. The measures reported here were recorded before (preintervention) and 2 wk after manipulation of the intermuscular connective tissues (postintervention). EMG and sonomicrometry signals were synchronously sampled and digitized by a common controller (Digital Sonomicrometer; Sonometrics, London, ON, Canada). Kinematic data and EMG-sonomicrometry signals from the implanted sensors were synchronized by an electronic trigger pulse to the sonomicrometry controller. Data from 15-s trials, each including at least 30 stride cycles, were collected during a single measurement session. Stride cycles from the same session were pooled to generate a single representative mean time series normalized to stride time for each animal and for pre- and postintervention conditions. Each measured variable was time normalized to the stride-cycle duration and averaged first within and then across rats.

Experimental Design

Animal training and sensor implantation. Five male Wistar rats (273 ± 15 g, body mass at the time of preintervention measurements) were trained to run in a Plexiglas-enclosed, motor-driven treadmill (Westra et al. 1985) for 10 days before implantation of sensors. Food rewards were provided upon completion of the 2-min running task at increasing speed (up to 0.8 m/s). During training and data collection days, rats were housed in large cages ($0.55 \times 0.33 \times 0.20$ m) with access to food and water ad libitum. Task and duration of task were as similar as possible between measurement sessions by applying 1-min recordings followed by 3- to 4-min rest for a maximum of ~15 min of recordings for each session per animal. This was necessary to exclude possible kinematic compensation of fatigue and for task with different mechanical demands. Recordings started after a 5-min warming-up phase before each measurement session. Because the presented data were collected at single points in time and the measurement procedures allowed for adaptation to treadmill speed before the kinematics recordings, we deemed intrasession variability and optimization on treadmill to be minimal. A detailed description of the surgical procedures for sensor implantation and for myofascial connective tissue enhancement was published previously (Bernabei et al. 2017a; Maas et al. 2009). Briefly, fine-wire EMG electrodes (25-μm uncoated diameter; 7SS-1T; Science Products, Hofheim, Germany) were implanted in the midregion of SO, LG, and MG muscle bellies of the right hindlimb, ~2 mm deep and ~1 mm apart. Electrode placement was verified by stimulation through the implanted wires during surgery as well as by dissection of the implanted muscles on the euthanized animal after data collection. Sonomicrometry crystals (1 mm; Sonometrics) were implanted near the proximal and distal aponeurosis of SO and LG to measure muscle belly lengths. EMG electrodes and sonomicrometry crystals were implanted on opposite sides of the muscle bellies with respect to the surgical mesh. No crystal or electrode was lying directly underneath the mesh; EMG and crystals cables ran outside the compartment at the most proximal and distal areas, while the mesh was placed centrally, at the SO-LG interface (Fig. 1*B*).

Connectivity manipulation surgery. After sensor implantation surgery, the animals were allowed to recover for 2 wk before the intermuscular connectivity manipulation surgery. In the latter, connective tissues between the dorsal side of the SO and the ventral side of LG + PL were blunt dissected and a tissue-integrating mesh ($n = 7$; Premilene mesh; B. Braun Melsungen) was sutured to the SO muscle over two-thirds of its muscle belly at the interface between SO, LG, and plantaris (PL) muscles. Attention was paid to prevent involvement of SO tendons and damage of the SO neurovascular tract, the latter running centrally between SO and LG muscle bellies. A small opening in the central region of the mesh was made to avoid contact with this tract. The distal portion of the biceps (accessory head) and posterior crural fascia, covering the distal myotendinous junctions of SO, LG, medial gastrocnemius, and PL as well as the Achilles tendon, were left intact. Detailed procedures for the tissue-integrating mesh implantation are reported in Bernabei et al. (2017a). Both survival surgeries were performed in aseptic conditions, using inhalation anesthesia (2–3% isoflurane) and a one-time preoperative subcutaneous injection of a painkiller (0.02 mg/kg; Temgesic; Schering-Plough, Maarssen, The Netherlands). Additional doses were given 1–2 days after the surgery if signs of pain were noticed. On completion of measurements, animals were euthanized with a pentobarbital overdose (Euthasol 20%) injected intracardially, followed by double-sided pneumothorax. After the surgical procedures for sensor implantation, animals were allowed to recover for 1 wk before data collection and before undergoing the surgery for manipulation of myofascial connectivity. During this week and during the interval between manipulation surgery and subsequent recording, animals were at rest in the cage.

Controls for sensor implant reliability and persistency of adaptation. In two additional age-matched animals (289 ± 12 g, body mass at time of first measurement), the fine-wire electrodes and sonomicrometry crystals were implanted with the same procedures described before. No manipulation of intermuscular connective tissues was performed, so that the locomotion data from these rats, collected at the same time points as the manipulated ones, could provide information on the isolated effects of the sensor implantation. All surgical and experimental procedures were approved by the Committee on the Ethics of Animal Experimentation at the Vrije Universiteit Amsterdam and in strict agreement with the guidelines and regulations concerning animal welfare and experimentation set forth by Dutch law.

Kinematics

Two-dimensional videos of treadmill locomotion were recorded with a high-speed camera (A602f; Basler, Ahrensburg, Germany). Markers placed on the iliac crest, greater trochanter, lateral femoral

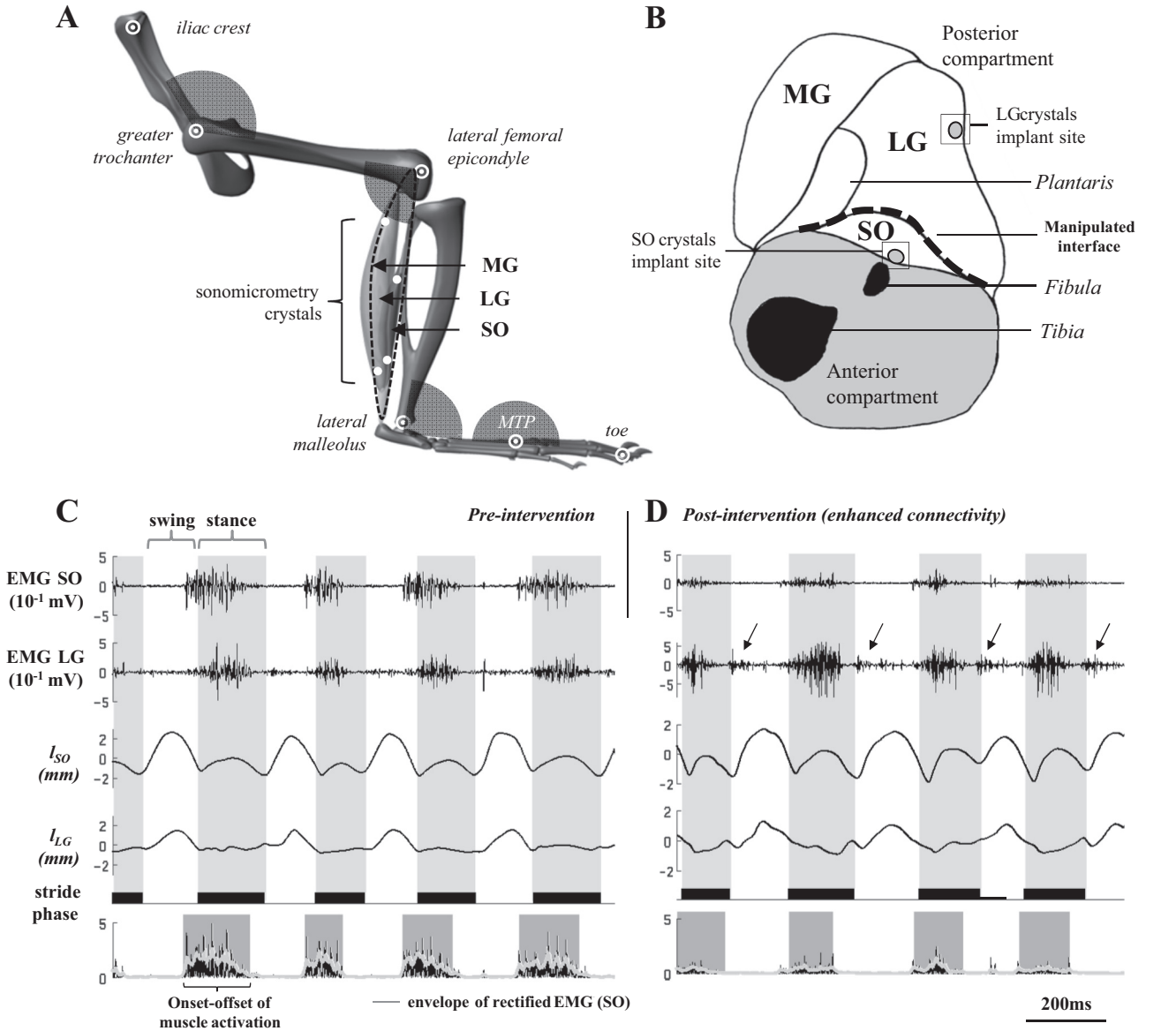

Fig. 1. Overview of data collection procedures. *A*: model of the rat hindlimb showing the motion tracking markers (open-white circles) on the selected anatomical markers and the convention for joint angles (grey areas). The closed-white circles indicate the position of the sonomicrometry crystals implanted in soleus (SO) and lateral gastrocnemius (LG). Medial gastrocnemius (MG) muscle tendon unit is indicated as a dotted perimeter. *B*: outline of cross section of the right hindlimb (based on schematics reported in Rijkelijkhuizen et al. 2007). The location of intermuscular connectivity manipulation (see METHODS) is shown (thick dashed line). *C* and *D*: representative raw electromyograms (EMG) and muscle lengths patterns of SO and LG simultaneously recorded during level trotting on a treadmill at an imposed speed of 0.8 m/s (*rat 1*). Signals were recorded from the same animal pre (*C*)- and postintervention (*D*). Stance (dark gray areas) and swing (white areas) phases of the right foot are highlighted. Black arrows indicate secondary activation bursts that were enhanced after mesh implantation. *Bottom*: EMG amplitude (black line: filtered-rectified EMG signal; light gray line: envelope of EMG signal) and the identification of EMG bursts (dark gray areas) on the SO EMG reported on top of the trace.

epicondyle, lateral malleolus, fifth metatarsophalangeal (MTP) joint, and the distal end of the fourth digit (Fig. 1*A*, white circles) were tracked to reconstruct the sagittal plane hindlimb kinematics. Skin movement artifacts were minimized by triangulating the position of the knee marker given the position of the great trochanter and lateral malleolus markers, and the lengths of femur and tibia were measured. Video data (400 × 180 pixels, 7.4 pixel/mm) were sampled at 200 frames/s, streamed to an IEEE-1394 port, and recorded to the computer hard drive with custom software (Labview; National Instruments, Austin, TX).

The duration of the stance and swing phases, as well as the stride length, was calculated using the time points of paw-in and paw-off, respectively, determined for each stride as *1*) the onset of the stance phase, defined as the video frame in which the foot of the hindlimb touched the treadmill belt; and *2*) the onset of the swing phase, defined as the video frame in which the same foot left the ground completely (Fig. 1*C*). The tracked anatomical landmarks were used to calculate the flexion-extension joint angle changes and range of motion (ROM) of hip, knee, ankle, and MTP over the stride.

Electromyography

During data collection, EMG signals from triceps surae muscles were amplified (100–2,000 times, common-mode rejection ratio >100 dB), filtered to prevent aliasing (10–1,000 Hz) and sampled (3,120 Hz). Band-pass and notch digital zero-lag filters were subse-

quently applied to remove movement artifacts (30–1,000 Hz, third-order Butterworth) and power-line interference (50 Hz, third-order Butterworth). Several descriptors of muscle activation were calculated as follows: *1*) the duration of the time-window between onset and offset of muscle activation (*burst duration*); *2*) the median value of the Fourier-decomposed frequency content of the burst (*burst median frequency*); *3*) the root-mean-squared (RMS) value of the rectified EMG burst (*burst amplitude*); and *4*) the *peak* value of the averaged envelope of the EMG signal across strides, computed as the maximum magnitude of the discrete-time analytic signal calculated by the Hilbert-transform (see Fig. 1, *C* and *D*, *bottom*). The amplitude of the EMG burst and envelope for each muscle and time bin was normalized to the maximum value of the EMG envelope across all time bins and to the maximum value of the mean EMG-RMS, respectively, recorded during the preintervention session. The onset-offset of muscle activation was determined by *k*-means cluster analysis applied on the band-pass filtered EMG signal (Den Otter et al. 2006), which corresponds to assigning values of the EMG amplitude to a user-defined number of clusters ($n = 3$), with the lowest cluster reflecting inactivity.

EMG-EMG loops. The envelope of muscle activation averaged over time-normalized strides was smoothened with a 19-samples moving average, and the slope of the EMG-EMG loop was used to describe the amplitude ratio between two pairs of muscles (SO-LG, SO-MG, and LG-MG). This slope was calculated as follows (Prilutsky et al. 1994):

$$K_{EMG} = \frac{(maxEMG_{SO} - minEMG_{SO})}{(maxEMG_{LG} - minEMG_{LG})}$$

where *maxEMG* and *minEMG* are the maximal and minimal values of the envelope of muscle activation for a given muscle.

Sonomicrometry

Muscle belly length was measured as the distance between the piezoelectric crystals implanted near the proximal and distal ends of SO and LG muscle bellies. For this, the elapsed time for the ultrasound wave to be transmitted by one crystal and received by the other as well as the speed of sound at which the wave travels in vertebrate skeletal muscles (1,580 m/s, Topp and O'Brien 2000) were used.

Time series describing the muscle belly length changes of SO (l_{SO}) and LG (l_{LG}) during locomotion (Fig. 1, *C* and *D*) were low-pass filtered (second-order Butterworth, 50-Hz cut-off) and subsequently normalized to the reference length (l_{REF}), defined as the mean of the maximum and minimum muscle belly lengths during the swing phase of the *preintervention* and of the *postintervention* conditions, to take muscle growth into account (Gabaldón et al. 2004). Positive changes indicated lengthening, while negative changes indicated shortening. They were calculated as the difference between the maximum and the minimum belly lengths during stance and swing, separately and expressed as a percentage of l_{REF}. Muscle belly velocity of length change of SO and LG was computed using the method of finite differences.

Statistics

Data from the preintervention and postintervention sessions were compared with a Wilcoxon signed rank test to assess effects of enhanced connectivity on muscle activation (peak amplitude, burst RMS amplitude, burst duration, and median frequency), joint ROM, muscle belly lengthening and shortening, and peak velocities during stance and swing phases of the stride. To retain statistical power given the small sample, we focused on the comparison between the preintervention/postintervention (2 wk) sessions, while using data from the control animals for interpreting adaptations observed in the experimental group and effects of sensor implantation only. In this context, the family-wise error was limited to two levels (within subjects: preintervention/post-2 wk). Quantitative descriptors of EMG amplitude and duration, as well as joint angle ROM and muscle belly shortening/lengthening, were extracted from the two unmanipulated animals, which were compared with independent samples *t*-test applied on preintervention/postintervention time-matched data. In this case, normality was tested for all groups with a Shapiro-Wilk test, while homogeneity of variance was verified with Levene's test. At least 15 stride cycles of constant speed trotting were analyzed for each rat and time point; galloping gaits and strides with forward-backward acceleration on the belt were excluded from the analysis. All statistical tests were performed using SPSS (v. 21; SPSS, Chicago, IL). In all statistical analysis, results were considered to be significant when $P < 0.05$. Variability of descriptors is expressed as SD.

RESULTS

Consistency of EMG and Kinematics of Hindlimb over Time

Following sensor implantation in the unmanipulated animals ($n = 2$), SO activation (burst amplitude) did not change ($P = 0.164$, $P = 0.475$) between measurement sessions which were time matched with the pre- and postintervention sessions of the manipulated group. LG burst amplitudes decreased only in one animal from 0.75 ± 0.17 to 0.62 ± 0.18 (-17.5%; $P < 0.001$). MG burst amplitude also decreased from 0.40 ± 0.24 to 0.36 ± 0.06 (-10.2%; $P < 0.001$) and from 0.66 ± 0.11 to 0.60 ± 0.16 (-9.9%; $P < 0.001$). During the same period, changes in flexion-extension ROM for hip, knee, and ankle joints were all within 1 SD, except for the MTP-joint peak extension, which decreased by $4.6 \pm 1.7°$ during swing. Peak lengthening during stance of both SO and LG muscle bellies, which could only be determined in one animal, was reduced from $5.7 \pm 2.9\%$ of l_{REF} to $2.4 \pm 1.8\%$ ($P = 0.002$) and from $15.8 \pm 7.0\%$ to $10.0 \pm 5.4\%$ ($P < 0.001$), respectively. During the swing phase, peak lengthening of SO and LG decreased from $21 \pm 1.4\%$ of l_{REF} to $18.5 \pm 2.4\%$ ($P = 0.005$) and from 46.8 ± 4.6 to $38.3 \pm 5.8\%$ ($P < 0.001$), respectively. Finally, peak shortening of LG muscle belly was reduced from 22.0 ± 4.6 to $18.5 \pm 3.0\%$ ($P = 0.034$) during stance phase and from 37.0 ± 5.3 to $30.4 \pm 6.7\%$ ($P = 0.001$) during swing phase. Test statistics are reported in Table 1.

Effects of Enhanced Intermuscular Connectivity on Hindlimb Kinematics

Hindlimb kinematics before the intervention were similar to previous data for treadmill locomotion in the rat (Bauman and Chang 2010; Thota et al. 2005). Changing the connectivity between SO and LG did not result in changes of spatiotemporal characteristics of treadmill locomotion (see Table 2). Also, the joint angle pattern, measured 2 wk after manipulation of intermuscular connective tissues, was qualitatively similar to the preintervention condition, with no significant changes in in peak joint angles in stance and swing (Fig. 2). Overall, these data indicate that little or no changes in kinematics resulted from the connectivity increase at the SO/LG interface.

Effects of Enhanced Intermuscular Connectivity on Activation Patterns and Burst Characteristics

SO muscle. The intermuscular connectivity enhancement resulted in a substantial decrease in mean SO activation: the

Table 1. *Overview of statistical analysis*

Test/Dependent Variable	Pre- and Postintervention	Statistic	*P* Value
Wilcoxon signed rank test			
Stance duration	x	$Z(5) = -0.135$‡	0.893
Swing duration	x	$Z(5) = -1.625$†	0.104
Stride length	x	$Z(5) = -0.677$†	0.498
Peak extension angle knee (stance)	x	$Z(5) = -0.405$†	0.686
Peak flexion angle knee (stance)	x	$Z(5) = -0.135$‡	0.893
Peak extension angle knee (swing)	x	$Z(5) = -0.405$†	0.686
Peak flexion angle knee (swing)	x	$Z(5) = -0.674$†	0.500
Peak extension angle knee (stance)	x	$Z(5) = -0.405$†	0.686
Peak flexion angle knee (stance)	x	$Z(5) = -0.944$†	0.345
Peak extension angle knee (swing)	x	$Z(5) = -0.135$†	0.893
Peak flexion angle knee (swing)	x	$Z(5) = -0.944$†	0.345
Peak extension angle hip (stance)	x	$Z(5) = -0.944$†	0.345
Peak flexion angle hip (stance)	x	$Z(5) = -0.674$†	0.500
Peak extension angle hip (swing)	x	$Z(5) = -0.944$†	0.345
Peak flexion angle hip (swing)	x	$Z(5) = -1.214$†	0.225
Peak extension angle MTP (stance)	x	$Z(5) = -0.674$†	0.500
Peak flexion angle MTP (stance)	x	$Z(5) = -0.813$†	0.416
Peak extension angle MTP (swing)	x	$Z(5) = -1.214$‡	0.225
Peak flexion angle MTP (swing)	x	$Z(5) = -1.214$‡	0.225
SO mean burst amplitude	x	$Z(5) = -2.023$†	0.043*
SO peak EMG envelope	x	$Z(5) = -2.023$†	0.043*
LG mean burst amplitude	x	$Z(5) = -2.023$†	0.043*
LG peak EMG envelope	x	$Z(5) = -2.023$†	0.043*
MG mean burst amplitude	x	$Z(4) = -2.023$†	0.043*
MG peak EMG envelope	x	$Z(4) = -1.826$†	0.068
LG secondary burst peak envelope	x	$Z(5) = -2.023$†	0.043*
MG secondary burst peak envelope	x	$Z(4) = -1.826$†	0.068
SO burst duration	x	$Z(5) = -0.813$†	0.416
LG burst duration	x	$Z(5) = -2.023$†	0.043*
MG burst duration	x	$Z(4) = -0.542$‡	0.588
SO burst median frequency	x	$Z(5) = -1.214$†	0.225
LG burst median frequency	x	$Z(5) = -0.944$†	0.345
MG burst median frequency	x	$Z(4) = -0.365$‡	0.715
SO-LG slope (stride)	x	$Z(5) = -2.023$†	0.043*
SO-LG slope (prestance)	x	$Z(5) = -2.023$†	0.043*
SO-MG slope (stride)	x	$Z(4) = -1.826$†	0.068
SO-MG slope (prestance)	x	$Z(4) = -1.461$†	0.144
LG-MG slope (stride)	x	$Z(4) = -1.826$‡	0.068
SO muscle belly lengthening (stance)	x	$Z(4) = 0.000$†	1.000
SO muscle belly lengthening (swing)	x	$Z(4) = -1.826$†	0.068
SO muscle belly shortening (stance)	x	$Z(4) = -1.826$‡	0.068
SO muscle belly shortening (swing)	x	$Z(4) = -1.826$‡	0.068
LG muscle belly lengthening (stance)	x	$Z(3) = -1.604$‡	0.109
LG muscle belly lengthening (swing)	x	$Z(3) = -1.604$†	0.109
LG muscle belly shortening (stance)	x	$Z(3) = 0.000$†	1.000
LG muscle belly shortening (swing)	x	$Z(3) = -1.069$‡	0.285
SO peak lengthening speed	x	$Z(4) = -0.730$†	0.465
SO peak shortening speed	x	$Z(4) = -1.826$†	0.068
LG peak lengthening speed	x	$Z(3) = -1.604$†	0.109
LG peak shortening speed	x	$Z(3) = -0.000$‡	1.000
Independent samples *t*-test			
SO mean burst amplitude	x	*R*1: $t(47) = -1.41$	0.164
		*R*2: $t(39) = 0.727$	0.475
SO burst duration	x	$t(47) = 1.985$	0.53
		$t(39) = -1.82$	0.76
LG mean burst amplitude	x	$t(51) = 0.954$	0.343
		$t(50) = 6.487$	<0.001*
LG burst duration	x	$t(51) = -3.46$	0.001*
		$t(50) = -6.40$	<0.001*
MG mean burst amplitude	x	$t(35) = -4.43$	<0.001*
		$t(43) = -11.8$	<0.001*
MG burst duration	x	$t(35) = -3.49$	0.002*
		$t(43) = 1.024$	0.312
SO peak lengthening stance		$t(26) = 3.49$	0.002*
SO peak shortening stance		$t(26) = -0.662$	0.514

Continued

Table 1. —*Continued*

Test/Dependent Variable	Pre- and Postintervention	Statistic	*P* Value
LG peak lengthening stance		$t(26) = 3.704$	0.001*
LG peak shortening stance		$t(26) = -2.233$	0.034
SO peak lengthening swing		$t(26) = 3.229$	0.005*
SO peak shortening swing		$t(26) = -0.443$	0.661
LG peak lengthening swing		$t(26) = 4.350$	<0.001*
LG peak shortening swing		$t(26) = -3.942$	0.001*

MTP, 5th metatarsophalangeal joint; SO, soleus; LG, lateral gastrocnemius; MG, medial gastrocnemius. *R*1 and *R*2: each value corresponds to one of the two control animals. *$P < 0.05$. †Based on negative ranks. ‡Based on positive ranks.

average normalized burst amplitude was decreased from 0.79 ± 0.02 preintervention to 0.38 ± 0.16 postintervention (52% of the normalized preintervention value; see Fig. 4*A*). Normalized peak activation of SO was reduced to 0.48 ± 0.06 of the preintervention value. Qualitatively, no substantial changes were observed in the pattern of activation of SO over the stride (Fig. 3*A*).

LG and MG muscles. In contrast to SO, the activation of LG and MG muscles was increased substantially 2 wk after the intervention (Fig. 3, *B* and *C*). The average burst amplitude increased from 0.66 ± 0.05 preintervention to 1.34 ± 0.27 postintervention for LG (103% of the normalized preintervention value, Fig. 4*A*) and from 0.65 ± 0.15 to 1.25 ± 0.50 for MG (92%). Normalized LG peak activation increased to 1.65 ± 0.55 with respect to the preintervention values but did not change for MG. For both gastrocnemii, the general pattern of activation was not affected by the intervention (Fig. 3, *B* and *C*). However, secondary additional or amplified activation bursts were observed with enhanced connectivity conditions: LG-MG EMG activity increased before paw-off and in the early swing phase (40–70% of stride). However, such increase was not expressed equally in all animals. Individual data are shown in Fig. 5. Intermuscular connective tissues enhancement did not affect burst duration and median frequency of SO and MG muscles (Fig. 4, *B* and *C*), while LG burst duration increased postintervention from 0.125 ± 0.017 to 0.145 ± 0.021 s.

The direction of the EMG loops between SO and LG changed substantially following connective tissues manipulation (Fig. 6*A* and Table 3). The slope decreased from 1.18 ± 0.10 to 0.35 ± 0.17 for SO-LG loop and from 1.85 ± 0.80 to 0.67 ± 0.54 for SO-MG loop between pre- and postintervention, respectively; however, this was not substantial between SO and MG. The slope of the EMG-EMG relationship for LG and MG did not change significantly: 1.61 ± 0.84 preintervention and 1.89 ± 0.48 postintervention. The slope of the SO-LG and SO-MG loops showed a preferential recruitment of SO in the preintervention condition, which was reversed or decreased after manipulation of intermuscular connectivity. All loops had a clockwise direction, which did not change between conditions, indicating that the order in which muscles were activated was preserved.

Table 2. *Spatiotemporal characteristics of locomotion*

	Stride Duration, ms	Stance Duration, ms	Swing Duration, ms	Stride Length, mm
Preintervention	252 ± 9	139 ± 10	114 ± 5	182 ± 12
Postintervention	255 ± 23	137 ± 14	119 ± 10	185 ± 19

Values are shown as means ± SD ($n = 5$). No significant differences were found between pre- and postintervention values.

Focusing on the prestance activation of SO-LG and SO-MG relations (from the minimal activation till the arrow, Fig. 6, *A* and *B*), onset of SO activation relative to LG and MG had a similar initial slope between pre- and postintervention conditions. With enhanced connectivity, SO activation saturated at a lower value, maintaining this fairly constant level while LG and MG activation steadily increased over the early stance phase. The net effect resulted in a more marked hysteresis of the SO-LG and SO-MG loops in the postintervention condition. Moreover, as previously mentioned, enhanced LG and MG activity was observed just before the swing phase (40–70% of stride time), after SO muscle became inactive. This resulted in a different coordination of activation for SO-MG and LG-MG in late stance between pre- and postintervention conditions.

These results show remarkable changes in the amplitude ratio, with little or no changes in the relative phase of activation between the triceps surae muscles, 2 wk following manipulation of intermuscular connective tissues. It should be noted that cross talk between SO and LG-MG would result in similar patterns of activation of these muscles instead of the ones observed here (asynchronous). Because similar patterns of activity were found for LG and MG, we cannot rule out the possibility that the recorded activity of LG and MG would partially be explained by cross talk between these muscles. Intramuscular bipolar electrodes gather information from a small number of motor units due to the rather small interelectrodes distance (<2 mm). However, cross talk between different neuromuscular compartments can occur when electrodes are placed at their boundaries (English and Weeks 1989); thus implant sites were chosen on the dorsal side of either LG or MG muscle bellies and as far as possible from each other (>5 mm) to minimize cross talk. The increased magnitude of LG and MG bursts seems to compensate for a reduced SO activation. In combination with the nearly unchanged hindlimb kinematics, this suggests that a new recruitment strategy was adopted by the central nervous system to cope with the changes in muscular organization.

Effects of Enhanced Intermuscular Connectivity on Muscle Belly Length Changes

Enhancement of intermuscular connectivity did not have a statistically significant effect on SO and LG muscle belly length changes during stance or swing phase; however, an overall decrease of peak lengthening and shortening for SO

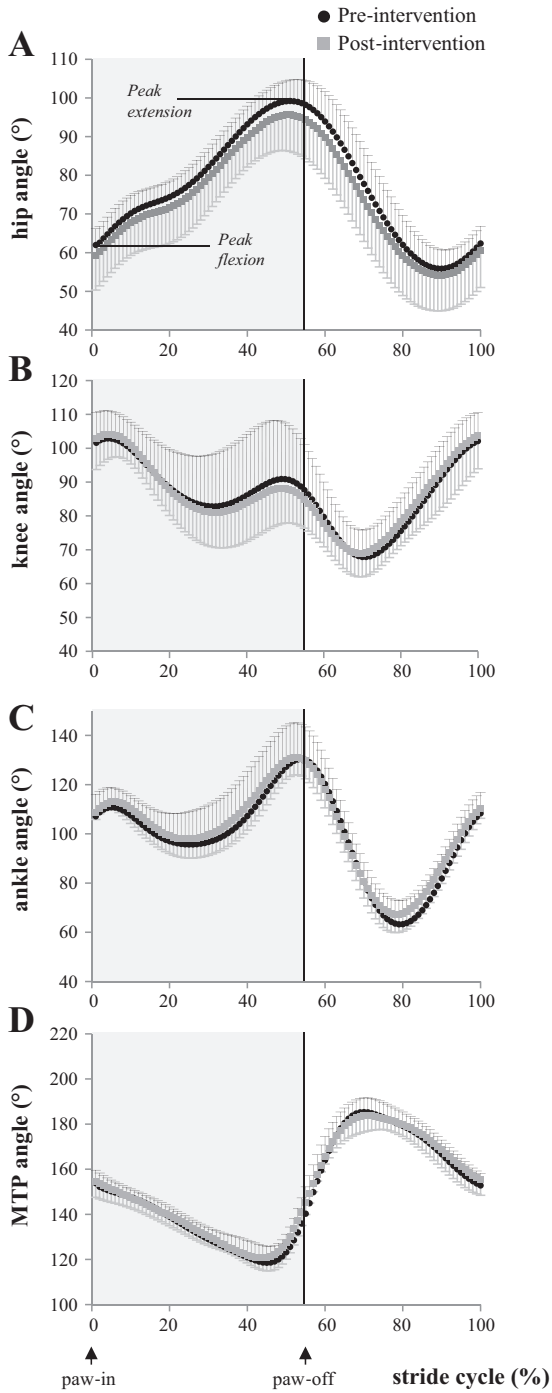

Fig. 2. Mean hindlimb joint angles during locomotion hip (*A*), knee (*B*), ankle (*C*), and metatarsophalangeal (MTP; *D*) angles during level trotting before (preintervention, means ± SD) and 2 wk after manipulation of intermuscular connective tissues (postintervention, means ± SD). Joint angles are plotted as a function of normalized stride cycle duration. Data were obtained from 5 animals. Treadmill speed was kept at 0.8 m/s in all conditions. Paw-in (*x*-axis origin) and paw-off (vertical line) of the right foot are indicated.

and LG was apparent postintervention (Table 4 and Fig. 7). Both are expressed as a percentage of l_{REF}. Muscle belly velocity was not affected by the connective tissues manipulation.

As a similar reduction in the contraction length range of SO and LG was found in one unmanipulated rat, this was likely not the result of the connective tissues manipulation. Therefore, these data do not indicate an effect on muscle belly length changes during locomotion of the increase of intermuscular connective tissues.

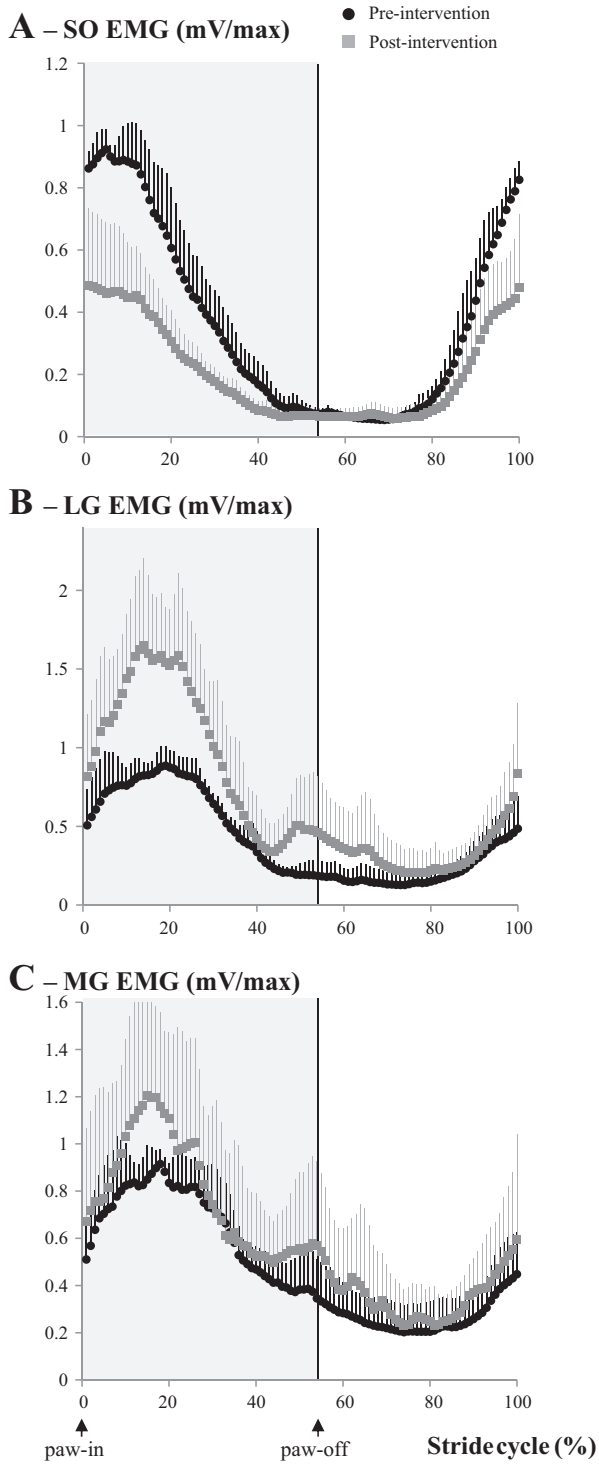

Fig. 3. Normalized EMG of soleus (SO), lateral (LG), and medial (MG) gastrocnemii muscles. Filtered rectified EMG envelope of SO, LG, and MG, normalized to the maximum amplitude measured in the preintervention condition, plotted as a function of normalized stride cycle duration. Means ± SD (n = 5) are compared before (preintervention) and after (postintervention) manipulation of intermuscular connectivity. Paw-in (*x*-axis origin) and paw-off (vertical line) of the right foot are indicated.

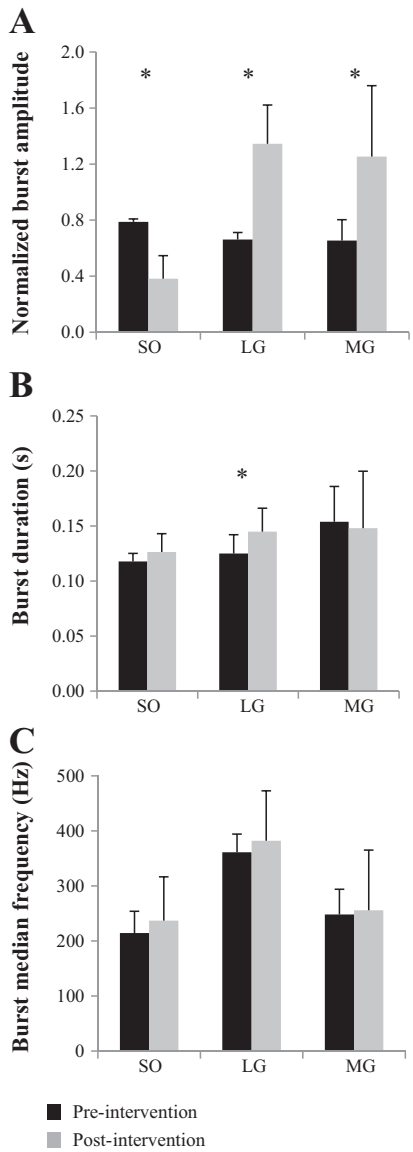

Fig. 4. EMG burst characteristics. EMG burst characteristics in the time and frequency domains before (preintervention) and after (postintervention) manipulation of intermuscular connective tissues for soleus (SO), lateral (LG), and medial (MG) gastrocnemii muscles. *A*: EMG burst mean-amplitude (RMS) normalized to the maximal amplitude obtained in the preintervention condition. *B*: absolute burst duration. *C*: median frequency of EMG burst. Data are shown as means ± SD ($n = 5$). Characteristics of EMG burst were compared pre- and postintervention ($*P < 0.05$).

DISCUSSION

The main finding of this study is that the coordinated activation of synergistic muscles during trotting changes as a consequence of enhanced intermuscular connectivity. We confirmed our first hypothesis that in response to an increased stiffness of the interface between SO and LG the neural drive of the targeted muscles is adapted to maintain normal movement. In contrast with our second hypothesis, muscle belly length during contraction did not seem to be affected by increased intermuscular connectivity.

We found that recruitment of individual muscles within the triceps surae synergistic group was substantially affected by mesh implantation. The neural drive to SO muscle was attenuated, while the neural drive to LG and MG muscles was increased. Changes in EMG of triceps surae muscles have been reported extensively. Previous studies have associated a shift of force sharing curves and ratios of muscle activation with variation in the mechanical demands required by diverse motor tasks (Hodson-Tole and Wakeling 2008; Hodson-Tole et al. 2012) and with task intensity, e.g., speed and slope (Hodgson 1983; Gregor et al. 2006; Kaya et al. 2003; Prilutsky et al. 1994). In contrast to the present results, the magnitude of SO and GA activity changed in the same direction. Selective inhibition of SO has been reported, but only during very specialized movements, such as paw-shaking in cats (Mehta and Prilutsky 2014; Smith et al. 1977, 1980). We observed small changes of hindlimb kinematics despite a different activation of triceps surae muscles. It should be noted that changes in hindlimb kinematics with changes in the joint torque produced by a single muscle is necessary only assuming no change in torques produced by all others synergistic and antagonistic muscles spanning the same joint. For instance, co-contraction of rectus femoris muscle may counteract a SO torque at the knee. We do not have information on the activation of antagonists, but we observed that LG and MG activation during trotting was increased after intervention, in contrast with a decrease of SO activation. Assuming a constant EMG-force relationship, different muscle activity could result in a reduced SO torque at the knee and an increased torque offered by gastrocnemii muscles. This scenario indicates that preservation of the kinematics pattern and hence of the joint torques was favored over conservation of muscles activation patterns.

Different mechanisms may explain the changes in SO-GA coordination observed in the present study. First, if recruitment of this muscle group was based solely on the size principle (Henneman 1957), the changes in intermuscular coordination would have required a substantial shift in fiber type composition between the pre- and postintervention conditions. This is deemed unlikely within the short time scale of the present study (2 wk). Moreover, we did not find differences in the median frequency of the EMG burst (Fig. 4*C*), which has been associated, although not without controversy (Kupa et al. 1995), with fiber type composition. In our experiment, the type of task and mechanical demand were unchanged, thus suggesting that the variation of SO, LG, and MG recruitment cannot be explained by the size principle.

Second, changes in sensory feedback in response to altered intermuscular connectivity may have affected muscle recruitment. In this study, muscle belly length was considered as a mechanical estimate of muscle spindle strain (Maas and Lichtwark 2009). A previous study by Smilde et al. (2016) reported a decreased force threshold and an increased length threshold of SO afferents in response to LG lengthening. As the effects of intermuscular connectivity depend on the length and relative position of neighboring muscles (Maas et al. 2004), these data suggest that an increase or decrease of such connectivity can be sensed by the central nervous system via length-dependent sensory feedback. However, in the present study we found similar muscle length over the stride after the intervention, in particular in the stance phase during which reflex-mediated activity can be expected. Although a decrease in the range of muscle belly shortening and lengthening is apparent between pre- and postintervention conditions, this was also found in nonmanipulated animals. Therefore, our data are insufficient to conclude that length feedback from spindle receptors of SO

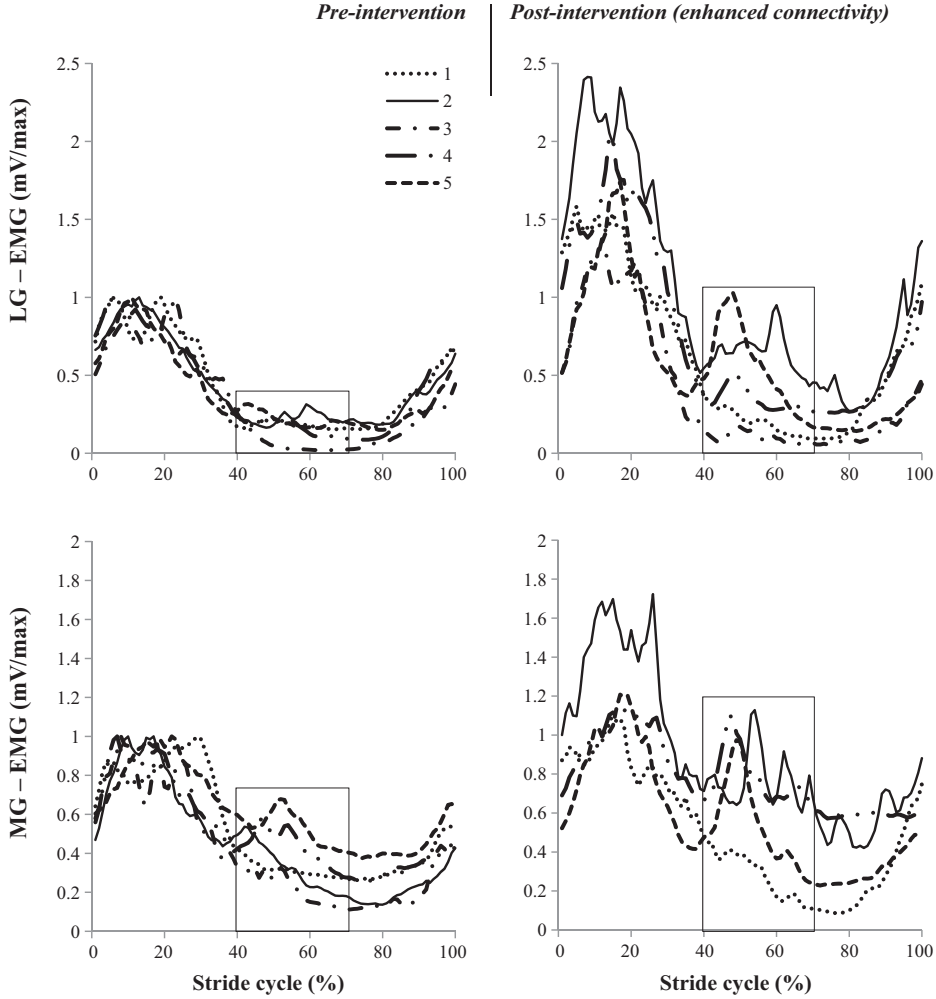

Fig. 5. Enhanced LG-MG muscle activity over the push-off phase. Preexistent muscle activation of LG and MG between 40 and 70% of the stride cycle was enhanced after implantation of the tissue integrating mesh. In most animals (*1*, *2*, *4*, and *5*), secondary EMG activity was present in late stance already before the intervention, while in one animal (*3*) no secondary bursts were apparent before intervention. The amplitude of this secondary burst was moderate relative to the main EMG burst during the stance phase. After intervention, the secondary burst was enhanced and appeared as a separate instance with respect to the main EMG burst. LG (*top*) and MG (*bottom*) EMG amplitudes were normalized to the maximal amplitude obtained in the preintervention condition. Time was expressed as a percentage of the stride cycle (%stride) ($n = 5$). For EMG MG postintervention, $n = 4$.

and LG was not affected by the connectivity enhancement. However, we did not measure tendon forces of individual triceps surae muscles and thus cannot exclude a potential role of Golgi tendon organs. Moreover, changes in amplitude and frequency of EMG of a muscle do not rely on autogenic length-feedback only but can be mediated also by altered length-feedback from neighboring muscles (Nichols et al. 2016; Pantall et al. 2016). In the present study, changes in length-feedback on SO and LG from neighboring muscles, i.e., MG and plantaris, cannot be excluded, although the lack of change in joint kinematics makes it unlikely. In addition, reflex-driven mechanisms may have affected the activation pattern changes observed here as a consequence of fascial pain and strain effects. Previous studies have considered the muscular fascia for its ability to alter the activation of nerve receptors by adapting its mechanical and viscoelastic properties, sensitivity to stress, and load resistance (Schleip et al. 2012; Turvey and Fonseca 2014). An increase in fascial stiffness, thus mimicking the connectivity enhancement adopted here, has been found to contribute to myofascial pain. This is common in a number of global and focal conditions including spastic palsy after stroke, rheumatoid arthritis, and contractures associated with past or present inflammatory processes (for a review, see Klingler et al. 2014). In fact, an abnormal thickening of perineural fascial tissues may lead to compression and stenosis of the nerve, thus involving partial or total loss of function, pain, a decreased haptic perception, loss of muscle force, and muscle atrophy. As thickening of the crural fascia and an increased stiffness of the intermuscular connective tissues were observed after implantation of the tissue-integrating mesh between SO and LG muscles in the rat (Bernabei et al. 2016), these factors need to be taken into account when interpreting the adaptation of muscle activation reported here.

Third, changes in interjoint coordination of one-joint vs. two-joint muscles can be the result of minimization of muscle stress and/or metabolic costs (Prilutsky 2000). It has been shown that selective inhibition of SO and changes in the ratio of activation between SO and MG can be obtained with different ankle-knee moments combinations after removal of velocity-dependent sensory feedback (Mehta and Prilutsky 2014). During stance in level locomotion, an ankle extension moment and a knee extension moment are required (Bennett et al. 2012; Kaya et al. 2003). As the two-joint GA also produces a flexion moment at the knee, such mechanical demands favors activation of the one-joint SO. We have shown previously that a substantial amount of force can be transmitted between SO and LG if these muscles are more tightly linked to each other (Bernabei et al. 2016, 2017a). For some relative muscle positions, part of the force produced by SO muscle fibers was found to be exerted at LG proximal tendon. In vivo, this would result in SO muscle producing a moment at the knee joint, thereby altering its role from a one-joint to a two-joint

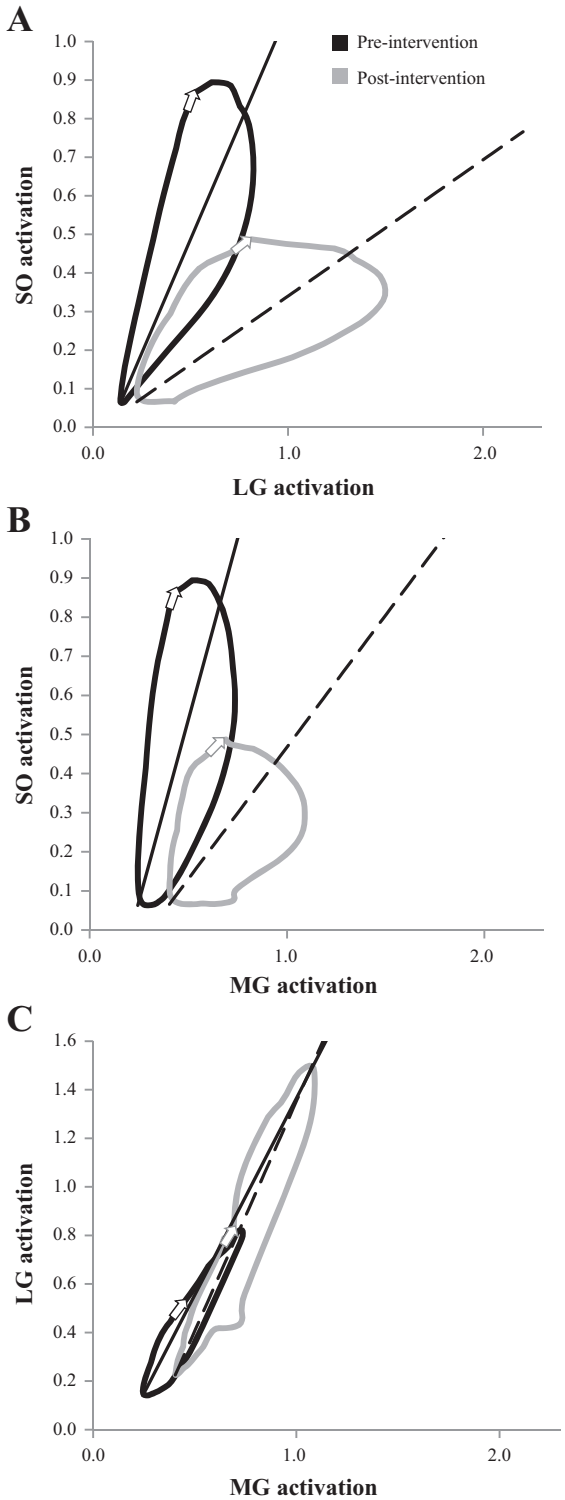

Fig. 6. Intermuscular coordination. Normalized EMG amplitude of one muscle is plotted as a function of normalized EMG amplitude of another muscle ($n = 5$). Values are normalized to the maximal amplitude obtained in the preintervention condition. *A*: SO-LG. *B*: SO-MG. *C*: LG-MG. Coordination of activation is compared before (black loop) and after manipulation of intermuscular connective tissues (gray loop). Regression lines for each coordination loop are shown (preintervention: solid line, postintervention: dashed line). Arrows indicate the paw-in event and the direction of the EMG-EMG loop.

Table 3. *Slope of muscle recruitment curves*

	Preintervention	Postintervention
SO-LG	1.18 ± 0.10	0.35 ± 0.17†
SO-MG	1.85 ± 0.80	0.67 ± 0.54*
LG-MG	1.61 ± 0.84	1.89 ± 0.48

Values are shown as means ± SD ($n = 5$). *$P < 0.05$; †$P < 0.01$ for pre- and postintervention comparison.

muscle. Furthermore, this would reduce the relative advantage for recruiting SO during the stance phase of trotting. Note, however, that tendon forces or joint torques were not measured in the present study. When considering multi-joint tasks, it seems reasonable that recruitment strategies would consider global state variables, e.g., combined joint moments, associated with the higher hierarchical level of muscle synergies instead of local ones, e.g., individual muscle conditions (Ting and McKay 2007). For instance, model predictions in humans show that for tasks with simultaneous knee-ankle flexion-extension, e.g., vertical jumps, the two-joint muscles LG and MG are mechanically advantageous (Prilutsky et al. 1994, 1996), requiring lower muscle stress and total force than if a combination of one-joint muscles will be used. However, the change in mechanical effect of SO does not explain the increased activity of LG and MG muscles. Because SO and GA are mechanically similar following the connectivity manipulation, other muscle characteristics may become important in the optimization of motor control. Our results may suggest that the central nervous system preferentially recruits the muscle with the highest physiological cross-sectional area, which is in agreement with minimizing stress and activation. If the changes in neuromuscular control observed here were a consequence of turning a one-joint muscle into a (partially) two-joint muscle, as supported by previous in situ experiments, it is conceivable that in the healthy state the central nervous system takes the moments muscles produce at the joints into account when optimizing motor control.

Limitations of this Study

Nonspecific effects of the connectivity enhancement surgery, such as pain-induced disuse and hindlimb unloading, cannot be excluded because no sham-operated group was tested. Such a design was not deemed to be representative of an intact connective tissue case, as it would involve, besides

Table 4. *Maximal shortening and lengthening of SO and LG muscle bellies*

	Max Lengthening: Stance, %	Max Shortening: Stance, %	Max Lengthening: Swing, %	Max Shortening: Swing, %
SO				
Preintervention	11.0 ± 5.6	−11.1 ± 8.7	35.1 ± 16.9	−30.1 ± 5.9
Postintervention	9.9 ± 4.1	−7.1 ± 5.9	20.7 ± 14.4†	−19.1 ± 12.0*
LG				
Preintervention	4.5 ± 4.8	−3.5 ± 2.3	14.6 ± 3.1	−12.9 ± 6.0
Postintervention	2.7 ± 1.0	−2.2 ± 0.6	9.4 ± 2.3*	−6.6 ± 2.2

Values are expressed as a percentage of reference length (l_{REF}) and shown as means ± SD ($n = 4$). Max, maximal. *$P < 0.05$; †$P < 0.01$ for pre- and postintervention comparison.

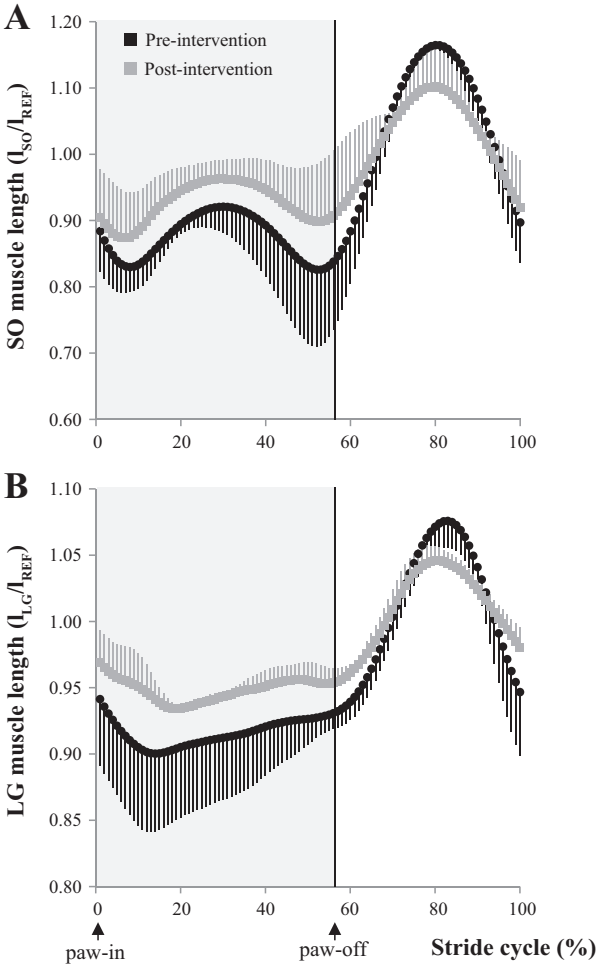

Fig. 7. Muscle belly length changes of soleus (SO) and lateral gastrocnemius (LG) muscles. Muscle belly lengths l_{SO} of SO (*A*) and l_{LG} of LG (*B*) normalized to the reference length of each muscle l_{REF}, defined as the mean of the maximum and minimum lengths in swing during level trotting for each animal. Normalized muscle belly lengths are expressed as a function of normalized stride cycle duration (%stride) with intact (preintervention, black circles, means ± SD, $n = 5$) and enhanced connectivity (postintervention, gray squares, means ± SD, $n = 4$). Paw-in (*x*-axis origin) and paw-off (vertical line) of the right foot are indicated.

cutting the skin and the compartmental fascia, also removing the connective tissues linkages between SO and LG. This intervention and subsequent tissue remodeling at the SO and LG interface could then also alter the mechanical interaction between these muscles. In a previous paper (Bernabei et al. 2017a), we have shown that no differences in mechanical interaction between SO and LG + PL and controls are observed when implanting an adhesion-barrier mesh, which is similar to a sham surgery without subsequent remodeling of intermuscular connective tissues. However, we also showed that the mass of triceps surae muscles did not change following mesh implantation (Bernabei et al. 2016), while this would be expected following denervation (Kobayashi et al. 1997). In addition, we previously observed a decrease of SO and LG + PL forces, consistent with a weakened triceps surae following manipulation surgery (Bernabei et al. 2017a). Given the similar kinematic pattern of the hindlimb observed here, and assuming similar weight bearing, an increase in activation of all plantarflexors would be expected. However, in our experiment only LG and MG activation increased (EMG from PL was not measured). Therefore, the decrease of SO muscle activation does not seem to be directly related to a generalized loss of muscle force, but it may rather indicate a selective change of muscle activation. Finally, when implanted in between muscles, the surgical mesh may restrain SO muscle belly during relaxation and cause SO force reduction. This is because the mesh was originally devised for hernia and thoracic wall repair, thus providing resistance when extended (axial stiffness: 7.7 to 20 N/mm; Novitsky et al. 2007). On the other hand, the flexural stiffness for the PREMILENE mesh used in this study was measured to be 0.018 N/mm (force couple to bend the mesh area in one unit of curvature), while we have previously reported that SO muscle can exert 1.2 to 1.5 N of force (within supramaximal stimulation) over a change in muscle belly length of ~8 mm measured during a locomotion stride (Bernabei et al. 2015, 2017b). Also, it should be noted that the mesh was sutured with loose connections (nonabsorbable suture wire) to the dorsal side of SO muscle only, with the muscle in a passive state (under anesthesia) and the ankle joint set at a dorsiflexed angle, so that restraining of the muscle due to the mesh mechanical resistance to dorsiflexion during locomotion and muscle growth would be minimal. Given the mechanical properties of the mesh and the procedures for implantation, we deem the stiffness of the mesh to be minimally affecting the force produced by SO and its activation. This was confirmed by similar to normal length-force curves collected in previous in situ experiments (Bernabei et al. 2015, 2016b).

Skin marker kinematics and two-dimensional motion data may limit the accuracy of the kinematic descriptors presented here. However, two-dimensional data obtained from X-ray motion tracking and bone-derived markers (Bauman and Chang 2010) yielded similar patterns of hindlimb joint angular motion in the sagittal plane. Moreover, Joãoa et al. (2010) reported that large differences between two-dimensional and three-dimensional motion data are found in the frontal and horizontal planes, while hip-knee-ankle flexion-extension during gait can be well approximated by the sagittal plane motion only. We estimated a maximum projection error of 17.9° and 17.5° for changes in knee and ankle joint angles, respectively, based on previously reported three-dimensional kinematics data of the rat hindlimb during walking (Thota et al. 2005).

Sonomicrometry crystals were implanted to measure changes in muscle belly strain in response to an increased mechanical coupling between SO and LG. However, several factors may have confounded these measures. First, the effect of growth on the distances between sonomicrometry crystal was taken into account by normalizing the SO and LG muscle belly lengths to the reference length pre- and postintervention (see METHODS). Second, dislodging of the crystals from their original site of implantation was evaluated by harvesting the muscles after euthanasia. Third, migration of the crystals was tested by comparison with nonmanipulated animals. Indeed, one control animal showed similar changes in SO and LG muscle belly length changes as for the manipulated group. This means that the observed decrease in SO and LG muscle belly length changes cannot be ascribed to interferences with the mesh. A larger sample size is needed to identify more subtle differences in muscle belly length changes with altered myofascial connectivity.

The reliability of sonomicrometry and EMG data over time was evaluated by collecting data from two animals that underwent surgery for sensor implantation only. Monitoring changes in the signals acquired via the chronic implant revealed that EMG patterns from target muscles could be reliably collected up to 6 wk after implantation, as previously reported in a similar experiment in mice (Tysseling et al. 2013). However, longitudinal data collection involving sonomicrometry crystals was more challenging, as changes in the recorded sonomicrometry distances occurred 2 wk after the first measurement with no known alteration of the implant environment. Also, dislodging of crystals was found after euthanasia and muscle harvesting in one control animal.

ACKNOWLEDGMENTS

We thank Guus Baan and Wendy Noort for assistance with training the rats and data collection. We thank Frans den Boer for designing and building the implantable connectors, as well as Bert Coolen for technical assistance for high-speed kinematics recordings. We further thank Maike Visschedijk and Julie Teeuwen for helping with the motion tracking analysis.

GRANTS

This study was supported by the Division for Earth and Life Sciences of the Netherlands Organization for Scientific Research (864-10-011 to H. Maas).

DISCLOSURES

No conflicts of interest, financial or otherwise, are declared by the authors.

AUTHOR CONTRIBUTIONS

H.M. conceived and designed research; M.B. performed experiments; M.B. analyzed data; M.B., J.H.v.D., and H.M. interpreted results of experiments; M.B. prepared figures; M.B. drafted manuscript; M.B., J.H.v.D., and H.M. edited and revised manuscript; M.B., J.H.v.D., and H.M. approved final version of manuscript.

REFERENCES

Bauman JM, Chang YH. High-speed X-ray video demonstrates significant skin movement errors with standard optical kinematics during rat locomotion. *J Neurosci Methods* 186: 18–24, 2010. doi:10.1016/j.jneumeth.2009.10.017.

Bennett SW, Lanovaz JL, Muir GD. The biomechanics of locomotor compensation after peripheral nerve lesion in the rat. *Behav Brain Res* 229: 391–400, 2012. doi:10.1016/j.bbr.2012.01.040.

Bernabei M, van Dieën JH, Maas H. Altered mechanical interaction between rat plantar flexors due to changes in intermuscular connectivity. *Scand J Med Sci Sport* 27: 177–187, 2017a. doi: 10.1111/sms.12644.

Bernabei M, van Dieën JH, Maas H. Longitudinal and transversal displacements between triceps surae muscles during locomotion of the rat. *J Exp Biol* 220: 537–550, 2017b. doi:10.1242/jeb.143545.

Bernabei M, Maas H, van Dieën JH. A lumped stiffness model of intermuscular and extramuscular myofascial pathways of force transmission. *Biomech Model Mechanobiol* 15: 1747–1763, 2016. doi:10.1007/s10237-016-0795-0.

Bernabei M, van Dieën JH, Maas H. Enhanced muscle connectivity changes neural control of synergistic muscles during locomotion. Society for Neuroscience 2015. Chicago, IL: 17–21 October 2015.

Bojsen-Møller J, Schwartz S, Kalliokoski KK, Finni T, Magnusson SP. Intermuscular force transmission between human plantarflexor muscles in vivo. *J Appl Physiol (1985)* 109: 1608–1618, 2010. doi:10.1152/japplphysiol.01381.2009.

Den Otter AR, Geurts AC, Mulder T, Duysens J. Gait recovery is not associated with changes in the temporal patterning of muscle activity during treadmill walking in patients with post-stroke hemiparesis. *Clin Neurophysiol* 117: 4–15, 2006. doi:10.1016/j.clinph.2005.08.014.

Donelan JM, Pearson KG. Contribution of force feedback to ankle extensor activity in decerebrate walking cats. *J Neurophysiol* 92: 2093–2104, 2004. doi:10.1152/jn.00325.2004.

English AW, Weeks OI. Electromyographic cross-talk within a compartmentalized muscle of the cat. *J Physiol* 416: 327–336, 1989.

Gabaldón AM, Nelson FE, Roberts TJ. Mechanical function of two ankle extensors in wild turkeys: shifts from energy production to energy absorption during incline versus decline running. *J Exp Biol* 207: 2277–2288, 2004. doi:10.1242/jeb.01006.

Gregor RJ, Smith DW, Prilutsky BI. Mechanics of slope walking in the cat: quantification of muscle load, length change, and ankle extensor EMG patterns. *J Neurophysiol* 95: 1397–1409, 2006. doi:10.1152/jn.01300.2004.

Henneman E. Relation between size of neurons and their susceptibility to discharge. *Science* 126: 1345–1347, 1957.

Hodgson JA. The relationship between soleus and gastrocnemius muscle activity in conscious cats–a model for motor unit recruitment? *J Physiol* 337: 553–562, 1983. doi:10.1113/jphysiol.1983.sp014641.

Hodson-Tole EF, Pantall A, Maas H, Farrell B, Gregor RJ, Prilutsky BI. Task-dependent activity of motor unit populations in feline ankle extensor muscles. *J Exp Biol* 215: 3711–3722, 2012. doi:10.1242/jeb.068601.

Hodson-Tole EF, Wakeling JM. Motor unit recruitment patterns 1: responses to changes in locomotor velocity and incline. *J Exp Biol* 211: 1882–1892, 2008. doi:10.1242/jeb.014407.

Huijing PA. Muscle as a collagen fiber reinforced composite: a review of force transmission in muscle and whole limb. *J Biomech* 32: 329–345, 1999. doi:10.1016/S0021-9290(98)00186-9.

Huijing PA, Baan GC. Extramuscular myofascial force transmission within the rat anterior tibial compartment: proximo-distal differences in muscle force. *Acta Physiol Scand* 173: 297–311, 2001. doi:10.1046/j.1365-201X.2001.00911.x.

Joãoa F, Amadoa S, Velosoa A, Armada-da-Silvaa P, Maurício AC. Anatomical reference frame versus planar analysis: implications for the kinematics of the rat hindlimb during locomotion. *Rev Neurosci* 21: 469–485, 2010.

Kaya M, Leonard T, Herzog W. Coordination of medial gastrocnemius and soleus forces during cat locomotion. *J Exp Biol* 206: 3645–3655, 2003. doi:10.1242/jeb.00544.

Klingler W, Velders M, Hoppe K, Pedro M, Schleip R. Clinical relevance of fascial tissue and dysfunctions. *Curr Pain Headache Rep* 18: 439, 2014. doi:10.1007/s11916-014-0439-y.

Kobayashi J, Mackinnon SE, Watanabe O, Ball DJ, Gu XM, Hunter DA, Kuzon WM. The effect of duration of muscle denervation on functional recovery in the rat model. *Muscle Nerve* 20: 858–866, 1997.

Kupa EJ, Roy SH, Kandarian SC, De Luca CJ. Effects of muscle fiber type and size on EMG median frequency and conduction velocity. *J Appl Physiol (1985)* 79: 23–32, 1995.

Maas H, Sandercock TG. Force transmission between synergistic skeletal muscles through connective tissue linkages. *J Biomed Biotechnol* 2010: 575672, 2010. doi:10.1155/2010/575672.

Maas H, Baan GC, Huijing PA. Intermuscular interaction via myofascial force transmission: effects of tibialis anterior and extensor hallucis longus length on force transmission from rat extensor digitorum longus muscle. *J Biomech* 34: 927–940, 2001. doi:10.1016/S0021-9290(01)00055-0.

Maas H, Baan GC, Huijing PA. Muscle force is determined also by muscle relative position: isolated effects. *J Biomech* 37: 99–110, 2004. doi:10.1016/S0021-9290(03)00235-5.

Maas H, Gregor RJ, Hodson-Tole EF, Farrell BJ, Prilutsky BI. Distinct muscle fascicle length changes in feline medial gastrocnemius and soleus muscles during slope walking. *J Appl Physiol (1985)* 106: 1169–1180, 2009. doi:10.1152/japplphysiol.01306.2007.

Maas H, Lichtwark GA. Is muscle-tendon unit length a valid indicator for muscle spindle output? *J Physiol* 587: 13–14, 2009. doi:10.1113/jphysiol.2008.165555.

Maas H, Sandercock TG. Are skeletal muscles independent actuators? Force transmission from soleus muscle in the cat. *J Appl Physiol (1985)* 104: 1557–1567, 2008. doi:10.1152/japplphysiol.01208.2007.

Mehta R, Prilutsky BI. Task-dependent inhibition of slow-twitch soleus and excitation of fast-twitch gastrocnemius do not require high movement speed and velocity-dependent sensory feedback. *Front Physiol* 5: 410, 2014. doi:10.3389/fphys.2014.00410.

Nichols RT, Bunderson NE, Lyle MA. Neural regulation of limb mechanics: insights from the organization of proprioceptive circuits. In: *Neuromechanical Modeling of Posture and Locomotion*. New York: Springer, 2016, p. 197–223.

Novitsky YW, Harrell AG, Cristiano JA, Paton BL, Norton HJ, Peindl RD, Kercher KW, Heniford BT. Comparative evaluation of adhesion formation, strength of ingrowth, and textile properties of prosthetic meshes after long-term intra-abdominal implantation in a rabbit. *J Surg Res* 140: 6–11, 2007. doi:10.1016/j.jss.2006.09.015.

Oda T, Kanehisa H, Chino K, Kurihara T, Nagayoshi T, Fukunaga T, Kawakami Y. In vivo behavior of muscle fascicles and tendinous tissues of human gastrocnemius and soleus muscles during twitch contraction. *J Electromyogr Kinesiol* 17: 587–595, 2007. doi:10.1016/j.jelekin.2006.04.013.

Pantall A, Hodson-Tole EF, Gregor RJ, Prilutsky BI. Increased intensity and reduced frequency of EMG signals from feline self-reinnervated ankle extensors during walking do not normalize excessive lengthening. *J Neurophysiol* 115: 2406–2420, 2016. doi:10.1152/jn.00565.2015.

Prilutsky BI. Coordination of two- and one-joint muscles: functional consequences and implications for motor control. *Mot Contr* 4: 1–44, 2000. doi:10.1123/mcj.4.1.1.

Prilutsky BI, Herzog W, Allinger TL. Force-sharing between cat soleus and gastrocnemius muscles during walking: explanations based on electrical activity, properties, and kinematics. *J Biomech* 27: 1223–1235, 1994. doi:10.1016/0021-9290(94)90276-3.

Prilutsky BI, Herzog W, Allinger TL. Mechanical power and work of cat soleus, gastrocnemius and plantaris muscles during locomotion: possible functional significance of muscle design and force patterns. *J Exp Biol* 199: 801–814, 1996.

Rijkelijkhuizen JM, Meijer HJ, Baan GC, Huijing PA. Myofascial force transmission also occurs between antagonistic muscles located within opposite compartments of the rat lower hind limb. *J Electromyogr Kinesiol* 17: 690–697, 2007. doi:10.1016/j.jelekin.2007.02.004.

Rossignol S, Dubuc R, Gossard JP. Dynamic sensorimotor interactions in locomotion. *Physiol Rev* 86: 89–154, 2006. doi:10.1152/physrev.00028.2005.

Schleip R, Duerselen L, Vleeming A, Naylor IL, Lehmann-Horn F, Zorn A, Jaeger H, Klingler W. Strain hardening of fascia: static stretching of dense fibrous connective tissues can induce a temporary stiffness increase accompanied by enhanced matrix hydration. *J Bodyw Mov Ther* 16: 94–100, 2012. doi:10.1016/j.jbmt.2011.09.003.

Silder A, Heiderscheit BC, Thelen DG, Enright T, Tuite MJ. MR observations of long-term musculotendon remodeling following a hamstring strain injury. *Skeletal Radiol* 37: 1101–1109, 2008. doi:10.1007/s00256-008-0546-0.

Silder A, Reeder SB, Thelen DG. The influence of prior hamstring injury on lengthening muscle tissue mechanics. *J Biomech* 43: 2254–2260, 2010. doi:10.1016/j.jbiomech.2010.02.038.

Sinkjaer T, Andersen JB, Ladouceur M, Christensen LO, Nielsen JB. Major role for sensory feedback in soleus EMG activity in the stance phase of walking in man. *J Physiol* 523: 817–827, 2000. doi:10.1111/j.1469-7793.2000.00817.x.

Smeulders MJ, Kreulen M, Hage JJ, Baan GC, Huijing PA. Progressive surgical dissection for tendon transposition affects length-force characteristics of rat flexor carpi ulnaris muscle. *J Orthop Res* 20: 863–868, 2002. doi:10.1016/S0736-0266(01)00181-4.

Smeulders MJ, Kreulen M. Myofascial force transmission and tendon transfer for patients suffering from spastic paresis: a review and some new observations. *J Electromyogr Kinesiol* 17: 644–656, 2007. doi:10.1016/j.jelekin.2007.02.002.

Smilde HA, Vincent JA, Baan GC, Nardelli P, Lodder JC, Mansvelder HD, Cope TC, Maas H. Changes in muscle spindle firing in response to length changes of neighboring muscles. *J Neurophysiol* 115: 3146–3155, 2016. doi:10.1152/jn.00937.2015.

Smith JL, Betts B, Edgerton VR, Zernicke RF. Rapid ankle extension during paw shakes: selective recruitment of fast ankle extensors. *J Neurophysiol* 43: 612–620, 1980.

Smith JL, Edgerton VR, Betts B, Collatos TC. EMG of slow and fast ankle extensors of cat during posture, locomotion, and jumping. *J Neurophysiol* 40: 503–513, 1977.

Sokoloff AJ, Siegel SG, Cope TC. Recruitment order among motoneurons from different motor nuclei. *J Neurophysiol* 81: 2485–2492, 1999.

Stein RB, Misiaszek JE, Pearson KG. Functional role of muscle reflexes for force generation in the decerebrate walking cat. *J Physiol* 525: 781–791, 2000. doi:10.1111/j.1469-7793.2000.00781.x.

Thota AK, Watson SC, Knapp E, Thompson B, Jung R. Neuromechanical control of locomotion in the rat. *J Neurotrauma* 22: 442–465, 2005. doi:10.1089/neu.2005.22.442.

Tian M, Herbert RD, Hoang P, Gandevia SC, Bilston LE. Myofascial force transmission between the human soleus and gastrocnemius muscles during passive knee motion. *J Appl Physiol (1985)* 113: 517–523, 2012. doi:10.1152/japplphysiol.00111.2012.

Tijs C, van Dieën JH, Maas H. No functionally relevant mechanical effects of epimuscular myofascial connections between rat ankle plantar flexors. *J Exp Biol* 218: 2935–2941, 2015. doi:10.1242/jeb.122747.

Tijs C, van Dieën JH, Maas H. Limited in vivo mechanical effects of intermuscular myofascial connections within rat anterior crural compartment. *J Biomech* 49: 2953–2959, 2016. doi:10.1016/j.jbiomech.2016.07.005.

Ting LH, McKay JL. Neuromechanics of muscle synergies for posture and movement. *Curr Opin Neurobiol* 17: 622–628, 2007. doi:10.1016/j.conb.2008.01.002.

Topp KA, O'Brien WD Jr. Anisotropy of ultrasonic propagation and scattering properties in fresh rat skeletal muscle in vitro. *J Acoust Soc Am* 107: 1027–1033, 2000. doi:10.1121/1.428282.

Turvey MT, Fonseca ST. The medium of haptic perception: a tensegrity hypothesis. *J Mot Behav* 46: 143–187, 2014. doi:10.1080/00222895.2013.798252.

Tysseling VM, Janes L, Imhoff R, Quinlan KA, Lookabaugh B, Ramalingam S, Heckman CJ, Tresch MC. Design and evaluation of a chronic EMG multichannel detection system for long-term recordings of hindlimb muscles in behaving mice. *J Electromyogr Kinesiol* 23: 531–539, 2013. doi:10.1016/j.jelekin.2012.11.014.

Westra HG, de Haan A, van Doorn JE, de Haan EJ. The effect of intensive interval training on the anaerobic power of the rat quadriceps muscle. *J Sports Sci* 3: 139–150, 1985. doi:10.1080/02640418508729743.

Yaman A, Ozturk C, Huijing PA, Yucesoy CA. Magnetic resonance imaging assessment of mechanical interactions between human lower leg muscles in vivo. *J Biomech Eng* 135: 91003, 2013. doi:10.1115/1.4024573.